Electrochemical Fault Diagnosis for Lithium-Ion Batteries: Part 2 – Distributed Fault Diagnosis

Sara Sepasiahooyi and Shu-Xia Tang

***Abstract*— This paper presents a novel fault diagnosis framework for lithium-ion batteries in both the electrolyte and solid phases. The proposed scheme enables the detection, estimation, and isolation of electrochemical faults, including SEI film growth and lithium plating. This study consists of two parts, each of which can stand independently. Part 1 introduces the Single Particle Model with electrolyte dynamics integrated with side reactions (SPMe+SR), which serves as the battery model for this study, and proposes reformulated electrochemical fault models that facilitate the development of a fault diagnosis scheme. In this study, the proposed fault diagnosis scheme employs PDE backstepping cascaded observers, where the first estimates the distributed lithium concentration, and the second, an adaptive observer, estimates the fault magnitude via an update law. The effectiveness of the proposed approach is validated through simulations on a $LiFePO_4$ cell under an Urban Dynamometer Driving Schedule (UDDS) current profile.**

***Index Terms*— Lithium-ion battery; Fault detection; Fault estimation; Fault isolation; Degradation.**

I. Introduction

Faults are system malfunctions that degrade performance or cause failure. Therefore, early detection is essential for system safety and degradation monitoring. However, detecting internal faults in lithium-ion batteries remains challenging due to the complexity of their internal dynamics [1]. This study focuses on SEI film growth and lithium plating, which significantly affect battery performance. This study aims to detect, estimate, and isolate these faults. Electrochemical model–based fault diagnosis has been primarily developed for distributed thermal faults and degradation-related mechanisms. In [2], a pair of cascaded observers is proposed to identify and estimate the distributed temperature fault within a battery cell. Ferdowsi et al. [3] investigated faults in the solid-phase lithium concentration by developing PDE-based observers and using them to estimate the battery's remaining useful life. In [4], various electrochemical faults, such as reductions in the diffusion coefficient, variations in particle size and porosity, and electrical contact degradation, are diagnosed, isolated, and quantitatively estimated. This work develops two cascaded PDE backstepping observers to diagnose SEI film growth and lithium plating–related faults in both the electrolyte and solid phases. These mechanisms are particularly critical in high-energy-density applications such as electric vehicles, fast-charging systems, and grid-scale storage, where they can be triggered under high C-rate or low-temperature conditions, leading to capacity loss and safety risks. The main contributions of this work are:

- In [5], an electrolyte-phase fault diagnosis scheme for SEI degradation-induced faults was introduced. In this study, we extend that work to the solid phase by proposing a fault diagnosis scheme based on PDE backstepping cascaded observers, which include a state observer and a fault estimator.
- In [6], only the SEI film growth effect was considered. However, this study develops, to the best of our knowledge, the first model-based fault diagnosis framework capable of detecting and estimating both SEI growth and lithium plating.
- To the best of our knowledge, this is the first fault isolation scheme that determines whether a detected fault originates from SEI film growth or lithium plating by exploiting fault magnitude estimation.

In the remainder of this paper, Section II presents the battery model. Electrolyte- and solid-phase fault diagnosis are discussed in Sections III and IV, respectively. Fault isolation is addressed in Section V. Section VI reports simulation results, and Section VII concludes the paper with a summary and future directions.

S. Sepasiahooyi and S.-X. Tang (Corresponding author) are with the Department of Mechanical and Aerospace Engineering, Texas Tech University, Lubbock, TX, USA. ssepasia@ttu.edu, shuxia.tang@ttu.edu.

II. Battery Model

For the fault diagnosis scheme, the SPMe with incorporated Side-Reaction terms, denoted as SPMe+SR, is employed. This model relies on the key assumption that each electrode can be idealized as a single particle, as illustrated in Fig. 1. r and x denote the radial and spatial coordinates, respectively. The applied current $I(t)$ and terminal voltage $V(t)$ are the system's input and output, respectively. The

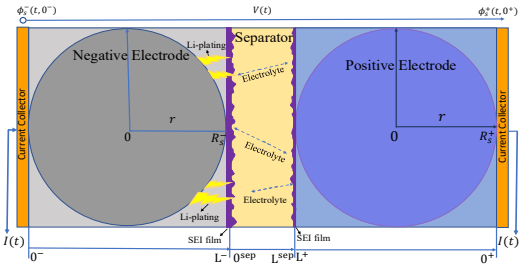

Fig. 1: Schematic of SPMe+SR.

solid-phase lithium concentration $c_s^{\pm}(t,r)$ dynamics and cor-

responding boundary conditions are given as:

$$\frac{\partial c_{\mathrm{s}}^{\pm}}{\partial t}(t,r) = \frac{1}{r^2}\frac{\partial}{\partial r}\left[D_{\mathrm{s}}^{\pm} r^2 \frac{\partial c_{\mathrm{s}}^{\pm}}{\partial r}(t,r)\right], \tag{1}$$

$$\frac{\partial c_{\mathrm{s}}^{\pm}}{\partial r}(t,0) = 0, \tag{2}$$

$$\frac{\partial c_{\mathrm{s}}^{\pm}}{\partial r}\left(t, R_{\mathrm{s}}^{\pm}\right) = \pm \frac{1}{D_{\mathrm{s}}^{\pm} F a_{\mathrm{s}}^{\pm} L^{\pm}} I(t) + \bar{f}_{\mathrm{s}}^{-}(t), \tag{3}$$

$$c_{\mathrm{s}}^{\pm}(0,r) = c_{\mathrm{s},0}^{\pm}(r), \tag{4}$$

where the specific interfacial area of the electrodes is given by $a_{\mathrm{s}}^{\pm} = \frac{3\varepsilon_{\mathrm{s}}^{\pm}}{R_{\mathrm{s}}^{\pm}}$. $\bar{f}_{\mathrm{s}}^{-}(t)$ represents a spatially uniform approximation of the solid-phase fault associated with lithium plating $\bar{f}_{\mathrm{s}}^{-}(t) = \bar{f}_{\mathrm{pl}}^{-}(t)$. The degradation-related side-reactions lead to local consumption or transfer of lithium within the electrode–electrolyte phases. From a mass conservation perspective, such degradation processes naturally appear as additive reaction terms in the diffusion equation. Therefore, the additive side-reaction structure adopted in this work follows directly from the conservation law formulation of lithium transport. The electrolyte-phase lithium concentration is governed by:

$$\frac{\partial c_{\mathrm{e}}^{\pm}}{\partial t}(t,x) = \frac{\partial}{\partial x}\left[\frac{D_{\mathrm{e}}^{\pm,\mathrm{eff}}(c_{\mathrm{e}}^{\pm}(t,x))}{\varepsilon_{\mathrm{e}}^{\pm}}\frac{\partial c_{\mathrm{e}}^{\pm}}{\partial x}(t,x)\right] \mp \frac{(1-t_c^0)}{\varepsilon_{\mathrm{e}}^{\pm} F L^{\pm}} I(t) + f_{\mathrm{e}}^{-}(t,x), \tag{5}$$

$$\frac{\partial c_{\mathrm{e}}^{sep}}{\partial t}(t,x) = \frac{\partial}{\partial x}\left[\frac{D_{\mathrm{e}}^{sep,\mathrm{eff}}(c_{\mathrm{e}}^{sep}(t,x))}{\varepsilon_{\mathrm{e}}^{sep}}\frac{\partial c_{\mathrm{e}}^{sep}}{\partial x}(t,x)\right], \tag{6}$$

where $f_{\mathrm{e}}^{-}(t,x)$ represents the electrolyte-phase fault associated with both SEI film growth and lithium plating $f_{\mathrm{e}}^{-}(t,x) = f_{\mathrm{SEI}}^{-}(t,x) + f_{\mathrm{pl}}^{-}(t,x)$. The electrolyte concentration PDEs (5) and (6) are subject to coupled boundary conditions. To address these interconnected PDEs, modified non-coupled boundary conditions are employed, as follows [7]:

$$\frac{\partial c_{\mathrm{e}}^{-}}{\partial x}(t,L^{-}) = \frac{-c_{\mathrm{e}}^{-}(t,L^{-})}{P^*}, \tag{7}$$

$$\frac{\partial c_{\mathrm{e}}^{+}}{\partial x}(t,L^{+}) = \frac{c_{\mathrm{e}}^{+}(t,L^{+})}{L^{\mathrm{sep}} - P^*}, \tag{8}$$

where $P^* = \frac{L^{+}+L^{\mathrm{sep}}-L^{-}}{2}$. The faults induced by SEI film growth and lithium plating are modeled as $f_i^{-}(t,x) = \theta_i \psi_i(t,x)$, $i \in \{\mathrm{SEI}, \mathrm{pl}\}$, as detailed in [8], where θ_i denotes the unknown fault magnitude and $\psi_i(t,x)$ denotes the known spatial distribution derived from the side-reaction kinetics. We assume a separation-of-variables representation for $\psi_i(t,x)$, which enables adaptive estimation of the unknown fault magnitude as

$$\psi_i(t,x) = \Omega_i(t - t_{i,\mathrm{fau}})\beta_i(x) c_{\mathrm{e}}^{-}(t,L^{-}), \tag{9}$$

where $\Omega_i(t - t_{i,\mathrm{fau}})$ is the fault time profile term:

$$\Omega_i(t - t_{i,\mathrm{fau}}) = \begin{cases} 0, & t < t_{i,\mathrm{fau}}, \\ 1 - e^{-a_i(t - t_{i,\mathrm{fau}})}, & t \geq t_{i,\mathrm{fau}}, \end{cases} \tag{10}$$

and $\beta_i(x)$ is defined as the spatial fault-rate profile

$$\beta_i(x) \triangleq \beta_i(0^{-}) + \frac{\beta_i(L^{-}) - \beta_i(0^{-})}{L^{-}} x. \tag{11}$$

The terminal voltage of the battery $V(t)$ is given by:

$$\begin{aligned} V(t) &= \frac{\mathrm{RT}}{\alpha F}\sinh^{-1}\left(\frac{-I(t)}{2a_{\mathrm{s}}^{+}L^{+}\bar{i}_0^{+}(t)}\right) \\ &- \frac{\mathrm{RT}}{\alpha F}\sinh^{-1}\left(\frac{I(t)}{2a_{\mathrm{s}}^{-}L^{-}\bar{i}_0^{-}(t)}\right) \\ &+ U^{+}\left(c_{\mathrm{ss}}^{+}(t)\right) - U^{-}\left(c_{\mathrm{ss}}^{-}(t)\right) \\ &- \left(\frac{R_f^{+}}{a_{\mathrm{s}}^{+}L^{+}} + \frac{R_f^{-}}{a_{\mathrm{s}}^{-}L^{-}} - \frac{L^{+} + 2L^{\mathrm{sep}} + L^{-}}{2\kappa_{\mathrm{e}}}\right) I(t) \\ &+ k_{\mathrm{conc}}(t)\left[\ln c_{\mathrm{e}}^{+}\left(t,0^{+}\right) - \ln c_{\mathrm{e}}^{-}\left(t,0^{-}\right)\right] \\ &\triangleq \nu_1\left(t, c_{\mathrm{ss}}^{\pm}(t), c_{\mathrm{e}}^{\pm}(t,0^{\pm}), I(t)\right), \end{aligned} \tag{12}$$

where $U^{\pm}(.)$ is the open circuit potential and $c_{\mathrm{ss}}^{\pm}(t) \triangleq c_{\mathrm{s}}^{\pm}(t, R_s^{\pm})$.

III. Electrolyte-phase fault diagnosis

In this section, two cascaded observers are designed for electrolyte-phase fault diagnosis. First, the electrolyte concentration is estimated by a state observer. Upon detection of an electrolyte-phase fault by the residual signal, the electrolyte-phase fault is estimated by a fault estimator.

A. Electrolyte-phase state observer

The electrolyte-phase observers are designed under the following assumption:

Assumption 1. *The electrolyte diffusion coefficient $D_e^{-}\left(c_e^{-}(t,x)\right)$ is assumed to be constant.*

To facilitate observer design, the electrolyte-phase lithium concentration dynamics are normalized using the following scales: $\bar{x} = \frac{x}{L^{-}}$ and $\bar{t} = \frac{D_{\mathrm{e}}^{-,\mathrm{eff}}}{(L^{-})^2 \varepsilon_{\mathrm{e}}^{-}} t$, resulting in the normalized system as follows:

$$\frac{\partial c_{\mathrm{e}}^{-}(\bar{t},\bar{x})}{\partial \bar{t}} = \frac{\partial^2 c_{\mathrm{e}}^{-}(\bar{t},\bar{x})}{\partial \bar{x}^2} + \frac{L^{-}\left(1 - t_{\mathrm{c}}^{0}\right)}{D_{\mathrm{e}}^{-,\mathrm{eff}} F} I(\bar{t}) + \theta_{\mathrm{e}}\psi_{\mathrm{e}}(\bar{t},\bar{x}), \tag{13}$$

$$\frac{\partial c_{\mathrm{e}}^{-}}{\partial \bar{x}}(\bar{t},0^{-}) = 0, \tag{14}$$

$$\frac{\partial c_{\mathrm{e}}^{-}}{\partial \bar{x}}(\bar{t},1^{-}) = -q^{-} c_{\mathrm{e},1}^{-}(\bar{t},1^{-}), \tag{15}$$

where $q^{-} = \frac{L^{-}}{P^*}$. The electrolyte state observer for normalized system (13)–(15) is proposed as follows:

$$\begin{aligned} \frac{\partial \hat{c}_{\mathrm{e},1}^{-}}{\partial \bar{t}}(\bar{t},\bar{x}) &= \frac{\partial^2 \hat{c}_{\mathrm{e},1}^{-}}{\partial \bar{x}^2}(\bar{t},\bar{x}) + \frac{L^{-}(1-t_c^0)}{D_{e}^{-,\mathrm{eff}} F} I(\bar{t}) \\ &+ \bar{k}_1(\bar{x})\left(c_{\mathrm{e}}^{-}(\bar{t},0^{-}) - \hat{c}_{\mathrm{e},1}^{-}(\bar{t},0^{-})\right), \end{aligned} \tag{16}$$

$$\frac{\partial \hat{c}_{\mathrm{e},1}^{-}}{\partial \bar{x}}(\bar{t},0^{-}) = \bar{k}_{10}\left(c_{\mathrm{e},1}^{-}(\bar{t},0^{-}) - \hat{c}_{\mathrm{e},1}^{-}(\bar{t},0^{-})\right), \tag{17}$$

$$\frac{\partial \hat{c}_{\mathrm{e},1}^{-}}{\partial \bar{x}}(\bar{t},1^{-}) = -q^{-}\hat{c}_{\mathrm{e},1}^{-}(\bar{t},1^{-}), \tag{18}$$

where $\bar{k}1(\bar{x})$ and $\bar{k}10$ are observer gains chosen such that $\hat{c}^-_{\mathrm{e},1}(\bar{t},\bar{x})$ converges to $c^-_{\mathrm{e}}(\bar{t},\bar{x})$ as $\bar{t}\to\infty$. The lithium concentration at the boundary $c^-_{\mathrm{e}}(\bar{t},0^-)$ can be obtained through measurable quantities such as the electrolyte diffusion coefficient, electrolyte conductivity, and electrolyte resistance, which can be measured using localized Electrochemical Impedance Spectroscopy (EIS), as detailed in [9]. Following the PDE backstepping observer design procedure, the kernel PDE system is derived as follows:

$$\frac{\partial^2\bar{k}}{\partial\bar{x}^2}(\bar{x},y)-\frac{\partial^2\bar{k}}{\partial y^2}(\bar{x},y)=-\alpha\bar{k}(\bar{x},y), \tag{19}$$

$$\frac{\partial\bar{k}}{\partial\bar{x}}(1,y)=-q^-\bar{k}(1,y), \tag{20}$$

$$\bar{k}(\bar{x},\bar{x})=-\frac{\alpha}{2}\bar{x}. \tag{21}$$

The solution of the kernel function is obtained as follows [6]:

$$\begin{aligned}\bar{k}(\bar{x},y)&=\frac{-\alpha q^-}{\sqrt{\alpha+(q^-)^2}}\\&\times\int_0^{\bar{x}-y}e^{q^-\tau/2}I_0(\sqrt{\alpha(2-\bar{x}-y)(\bar{x}-y-\tau)})\\&\times\sinh\left(\frac{\sqrt{\alpha+(q^-)^2}}{2}\tau\right)d\tau\\&-\alpha(1-y)\frac{I_1\left(\sqrt{\alpha\left((1-y)^2-(1-\bar{x})^2\right)}\right)}{\sqrt{\alpha\left((1-y)^2-(1-\bar{x})^2\right)}},\end{aligned} \tag{22}$$

where $I_m(\cdot)$ is the modified Bessel function of the first kind, and m denotes the order of the Bessel function [10, Appendix A.2]. Observer gains $k_1(\bar{x})$ and k_{10} are determined as:

$$\bar{k}_1(\bar{x})=-\bar{k}_y(\bar{x},0), \tag{23}$$

$$\bar{k}_{10}=-\frac{\alpha}{2}. \tag{24}$$

Theorem 1. *Consider the electrolyte dynamic system* (13)–(15) *and the designed state observer* (16)–(18)*. For any initial data, if $\alpha\geq\frac{1}{4}$, then, due to the invertibility of the backstepping transformation:*
1) In the absence of fault ($f_e^-(\bar{t},\bar{x})=0,\forall(\bar{t},\bar{x})\in[0,\infty)\times[0,1^-]$), the states of the state observer converge exponentially to the states of the system in the spatial L^2 norm.
2) In the presence of fault ($f_e^-(\bar{t},\bar{x})\neq0,\exists(\bar{t},\bar{x})\in[0,\infty)\times[0,1^-]$), the estimation error remains bounded.

Proof. Detailed proofs for both cases are provided in [2], with $\Delta_\omega Q(t,x)$ replaced by $f^-_{\mathrm{e}}(t,x)$. □

The electrolyte detection residual is defined as the estimation error of the electrolyte-phase state observer at the boundary, i.e.,

$$r_{\mathrm{e}}(t)=c^-_{\mathrm{e}}(t,L^-)-\hat{c}^-_{\mathrm{e},1}(t,L^-). \tag{25}$$

The fault residual does not become exactly zero in the absence of a fault due to modeling uncertainties. Therefore, the threshold level ϵ_{e} is chosen to be non-zero to account for uncertainty effects and to avoid false alarms using the probability of false alarm approach [2]. The system is fault-free when the residual signal satisfies $r_{\mathrm{e}}(t)<\epsilon_{\mathrm{e}}$. A fault is detected when the residual signal satisfies $r_{\mathrm{e}}(t)\geq\epsilon_{\mathrm{e}}$.

B. Electrolyte-phase fault estimator

Upon detection of an electrolyte-phase fault by the residual signal, the cascaded fault estimator is triggered. For fault estimation purposes, the electrolyte-phase fault is parameterized as

$$f^-_{\mathrm{e}}(t,x)=\theta_{\mathrm{e}}\psi_{\mathrm{e}}(t,x), \tag{26}$$

where θ_{e} denotes the unknown fault magnitude and $\psi_{\mathrm{e}}(t,x)$ denotes a known spatial distribution. Using the estimated electrolyte lithium concentration distribution $\hat{c}^-_{\mathrm{e},1}(\bar{t},\bar{x})$, produced by the state observer (16)-(18), the fault estimator is proposed as follows:

$$\begin{aligned}\frac{\partial\hat{c}^-_{\mathrm{e},2}}{\partial\bar{t}}(\bar{t},\bar{x})&=\frac{\partial^2\hat{c}^-_{\mathrm{e},2}}{\partial\bar{x}^2}(\bar{t},\bar{x})+\frac{L^-(1-t_c^0)}{D_e^{-,\mathrm{eff}}F}I(\bar{t})\\&+\hat{\theta}_{\mathrm{e}}\psi_{\mathrm{e}}(\bar{t},\bar{x})+k_2(\hat{c}^-_{\mathrm{e},1}(\bar{t},\bar{x})-\hat{c}^-_{\mathrm{e},2}(\bar{t},\bar{x})),\end{aligned} \tag{27}$$

$$\frac{\partial\hat{c}^-_{\mathrm{e},2}}{\partial\bar{x}}(\bar{t},0^-)=k_{10}\tilde{c}^-_{\mathrm{e},1}(\bar{t},0^-), \tag{28}$$

$$\frac{\partial\hat{c}^-_{\mathrm{e},2}}{\partial\bar{x}}(\bar{t},1^-)=-q^-\hat{c}^-_{\mathrm{e},1}(\bar{t},1^-), \tag{29}$$

where k_2 and k_{10} are estimator gains that will be determined to guarantee the stability of the estimation error system. The unknown term of the fault is estimated by the following adaptive law:

$$\dot{\hat{\theta}}_{\mathrm{e}}(\bar{t})=\frac{1}{k_3}\int_0^1\psi_{\mathrm{e}}(\bar{t},\bar{x})\tilde{c}_{\mathrm{e},3}(\bar{t},\bar{x})\,dx-\hat{\theta}_{\mathrm{e}}(\bar{t})\left\|\tilde{c}_{\mathrm{e},3}(\bar{t},\bar{x})\right\|, \tag{30}$$

where $k_3>0$ is to be chosen appropriately and $\tilde{c}^-_{\mathrm{e},3}(\bar{t},\bar{x})=\hat{c}^-_{\mathrm{e},2}(\bar{t},\bar{x})-\hat{c}^-_{\mathrm{e},1}(\bar{t},\bar{x})$, and $\|\cdot\|$ denotes the $L^2(0,1)$ norm.

Theorem 2. *Consider the electrolyte lithium concentration in* (13)–(15) *and the proposed estimator* (27)–(29) *with the update law given in* (30)*. If $k_2<\frac{1}{4}$ and $k_3>0$, then, under Assumption 1 for any initial data, the distributed state estimation error and the parameter estimation error $\tilde{\theta}(t)$ are ultimately bounded.*

Proof. The stability analysis is carried out using the Lyapunov function $W_2(\bar{t})=\frac{1}{2}\left\|\tilde{c}^-_{\mathrm{e},3}(\bar{t},\cdot)\right\|^2+\frac{k_3}{2}\left(\theta_{\mathrm{e}}-\hat{\theta}_{\mathrm{e}}(t)\right)^2$. Define $\boldsymbol{h}(t)=\left[\left\|\tilde{c}^-_{\mathrm{e},3}(t,\cdot)\right\|\quad\tilde{\theta}(t)\right]$, it can be concluded that:

$$\min\{1,k_3\}\|\boldsymbol{h}(t)\|^2\leqslant W_2(t)\leqslant\max\{1,k_3\}\|\boldsymbol{h}(t)\|^2.$$

By considering $\alpha_1(r)=\min\{1,k_3\}r^2$ and $\alpha_2(r)=\max\{1,k_3\}r^2$, based on [11, Section 4.8], if $k_2<\frac{1}{4}$, under one of the following conditions:

$$\|\tilde{c}_{\mathrm{e},3}(t,\cdot)\|\geq\frac{\delta\xi+\psi_{\max}\theta_{\max}+\frac{k_3}{4}\theta_{\max}}{\frac{1}{4}-k_2}:=\mu_1, \tag{31}$$

$$\left|\tilde{\theta}(t)\right|\geq\sqrt{\frac{\delta\xi+\psi_{\max}\theta_{\max}+\frac{k_3}{4}\theta^2_{\max}}{k_3}}+\frac{\theta_{\max}}{2}:=\mu_2, \tag{32}$$

the estimation error $\|\boldsymbol{h}(t)\|$ is ultimately bounded. $\xi := \max_{x\in[0,1]} k_1(x)$, and $\delta := \sup_{t\in[0,\infty)} \tilde{c}_{\mathrm{e},1}(t,0^-)$. Define

$$\mu = \left|\begin{bmatrix}\mu_1 & \mu_2\end{bmatrix}\right|, \tag{33}$$

where $|\cdot|$ denotes the 2-norm. Then, according to [11, Section 4.8], for every initial state $\boldsymbol{h}(0)$ satisfying

$$\|\boldsymbol{h}(0)\| \leq \alpha_2^{-1}\left(\alpha_1(r)\right),$$

there exists $T \geq 0$ (depending on $\boldsymbol{h}(0)$ and μ) such that

$$\|\boldsymbol{h}(\bar{t})\| \leq b = \alpha_1^{-1}(\alpha_2(\mu)) = \sqrt{\frac{\max\{1,k_3\}}{\min\{1,k_3\}}}\,\mu, \quad \forall \bar{t} \geq T.$$

□

The selection of the adaptive gain k_3 follows the analysis presented in [5].

IV. Solid-phase fault detection and estimation

For solid-phase fault diagnosis, a state observer is first designed to estimate the distributed lithium concentration. The availability of the surface lithium concentration $c_{\mathrm{ss}}^+(t)$, required for observer design, is first discussed. Subsequently, a fault estimator is developed to detect and estimate faults in the solid-phase lithium concentration.

A. Identification of surface lithium concentration $c_{ss}^+(t)$ via voltage function inversion

To design the solid-phase observer, the surface concentration $c_{\mathrm{ss}}^+(t)$ in the positive electrode is required. Since the voltage $V(t)$ and the electrolyte lithium concentrations at the terminal boundaries $c_{\mathrm{e}}^{\pm}(t,0^{\pm})$ are available, $c_{\mathrm{ss}}^+(t)$ can be obtained from the inversion of the voltage function $V(t)$. The total moles of lithium in the solid phase are given by [12]:

$$n_{\mathrm{Li},s}(t) = \sum_{j\in\{+,-\}} \frac{\varepsilon_{\mathrm{s}}^j L^j}{\frac{4}{3}\pi\left(R_{\mathrm{s}}^j\right)^3} \int_0^{R_{\mathrm{s}}^j} 4\pi r^2 c_{\mathrm{s}}^j(t,r)dr. \tag{34}$$

Assumption 2. *The total number of moles of lithium in the solid phase remains constant, i.e., $n_{\mathrm{Li},s}(t) = n_{\mathrm{Li},s}$.*

The average concentration is defined as $\bar{c}_{\mathrm{s}}^{\pm}(t) = \frac{3}{\left(R_{\mathrm{s}}^{\pm}\right)^3}\int_0^{R_{\mathrm{s}}^{\pm}} r^2 c_{\mathrm{s}}^{\pm}(t,r)\,\mathrm{d}r$. Under Assumption 2, one can obtain $\bar{c}_{\mathrm{s}}^-(t) = \rho\,\bar{c}_{\mathrm{s}}^+(t) + \beta$, where $\rho = -\frac{\varepsilon_{\mathrm{s}}^+ L^+}{\varepsilon_{\mathrm{s}}^- L^-}$, $\beta = \frac{n_{\mathrm{Li,s}}}{\varepsilon_{\mathrm{s}}^- L^-}$ [12]. By using polynomial solution profiles and the procedure presented in [13, Eq. (27)-(29)], the voltage function can be expressed as:

$$V(t) = \nu_2\left(t, c_{\mathrm{ss}}^+(t), c_{\mathrm{e}}^{\pm}(t,0^{\pm}), I(t)\right). \tag{35}$$

As long as (35) defines a one-to-one correspondence with respect to $c_{\mathrm{ss}}^+(t)$, uniformly in $I(t)$, the inversion of the voltage function can be derived. $c_{\mathrm{e}}^{\pm}(t,0^{\pm})$ can be obtained through other measurements using the EIS technique detailed in [9]. Consequently, given access to $c_{\mathrm{e}}^{\pm}(t,0^{\pm})$ and $V(t)$, the surface lithium concentration in the positive electrode, $c_{\mathrm{ss}}^+(t)$, can be determined as

$$c_{\mathrm{ss}}^+(t) = \nu_3\left(t, V(t), c_{\mathrm{e}}^{\pm}(t,0^{\pm}), I(t)\right). \tag{36}$$

B. Solid-phase state observer

Once a solid-phase fault is detected by the corresponding residual signal, the cascaded fault estimator is activated. The observer for estimating the solid-phase lithium concentration in the positive electrode is given in [12] as follows:

$$\frac{\partial \hat{c}_{\mathrm{s}}^+}{\partial t}(t,r) = D_{\mathrm{s}}^+\left[\frac{2}{r}\frac{\partial \hat{c}_{\mathrm{s}}^+}{\partial r}(t,r) + \frac{\partial^2 \hat{c}_{\mathrm{s}}^+}{\partial r^2}(t,r)\right] + \bar{p}_1^+(r)\left(c_{\mathrm{s}}^+(t,R_{\mathrm{s}}^+) - \hat{c}_{\mathrm{s}}^+(t,R_{\mathrm{s}}^+)\right), \tag{37}$$

$$\frac{\partial \hat{c}_{\mathrm{s}}^+}{\partial r}(t,0) = 0, \tag{38}$$

$$\frac{\partial \hat{c}_{\mathrm{s}}^+}{\partial r}\left(t,R_{\mathrm{s}}^+\right) = \frac{I(t)}{D_{\mathrm{s}}^+ F a_{\mathrm{s}}^+ L^+}, + \bar{p}_0^+(t)\left(c_{\mathrm{s}}^+(t,R_{\mathrm{s}}) - \hat{c}_{\mathrm{s}}^+(t,R_{\mathrm{s}})\right), \tag{39}$$

where the observer gains are computed as follows:

$$\bar{p}_1^+(r) = \frac{-\lambda D_{\mathrm{s}}^+}{2R_{\mathrm{s}}^+\bar{z}}\left[I_1(\bar{z}) - \frac{2\lambda}{\bar{z}}I_2(\bar{z})\right], \tag{40}$$

$$\bar{p}_0^+ = \frac{1}{2R_{\mathrm{s}}^+}(3-\lambda), \quad \text{for } \lambda < \frac{1}{4}, \tag{41}$$

where $\bar{z} = \sqrt{\lambda\left(\frac{r^2}{\left(R_{\mathrm{s}}^+\right)^2} - 1\right)}$. The observer for estimating the solid-phase lithium concentration in the negative electrode, based on the fault-integrated system, is designed as:

$$\frac{\partial \hat{c}_{\mathrm{s},1}^-}{\partial t}(t,r) = D_{\mathrm{s}}^-\left[\frac{2}{r}\frac{\partial \hat{c}_{\mathrm{s},1}^-}{\partial r}(t,r) + \frac{\partial^2 \hat{c}_{\mathrm{s},1}^-}{\partial r^2}(t,r)\right] + \bar{p}_1^-(r)\left(c_{\mathrm{s}}^+(t,R_{\mathrm{s}}^+) - \hat{c}_{\mathrm{s}}^+(t,R_{\mathrm{s}}^+)\right), \tag{42}$$

$$\frac{\partial \hat{c}_{\mathrm{s},1}^-}{\partial r}(t,0) = 0, \tag{43}$$

$$\frac{\partial \hat{c}_{\mathrm{s},1}^-}{\partial r}\left(t,R_{\mathrm{s}}^-\right) = \frac{I(t)}{D_{\mathrm{s}}^- F a_{\mathrm{s}}^- L^-} + \bar{p}_0^-\left(c_{\mathrm{s}}^+(t,R_{\mathrm{s}}^+) - \hat{c}_{\mathrm{s}}^+(t,R_{\mathrm{s}}^+)\right), \tag{44}$$

where the observer gains are:

$$\bar{p}_0^- = \frac{-1}{2R_{\mathrm{s}}^+}\frac{a_{\mathrm{s}}^+ L^+ D_{\mathrm{s}}^+}{a_{\mathrm{s}}^- L^- D_{\mathrm{s}}^-}(3-\lambda), \tag{45}$$

$$\bar{p}_1^-(r) = \frac{a_{\mathrm{s}}^+ L^+ \lambda D_{\mathrm{s}}^+}{2\left(R_{\mathrm{s}}^+\right)^3 \varepsilon_{\mathrm{s}}^- L^-} \times \int_0^{R_{\mathrm{s}}^+} \frac{r^2 \bar{p}_1^+(r)}{\bar{z}}\left[I_1(\bar{z}) - \frac{2\lambda}{\bar{z}}I_2(\bar{z})\right] dr. \tag{46}$$

For solid-phase observer design, it is assumed that $n_{\mathrm{Li,s}}$ is known and the initial estimates satisfy

$$n_{\mathrm{Li},s} = \sum_{j\in\{+,-\}} \frac{\varepsilon_s^j L^j}{\frac{4}{3}\pi (R_s^j)^3} \int_0^{R_s^j} 4\pi r^2 \hat{c}_s^j(0,r)\,dr. \tag{47}$$

If the initial concentration estimates are assumed to be uniform in r, then (47) simplifies to:

$$n_{\mathrm{Li,s}} = \varepsilon_s^+ L^+ \hat{c}_{\mathrm{s},0}^+ + \varepsilon_s^- L^- \hat{c}_{\mathrm{s},0}^-. \tag{48}$$

Theorem 3. *Consider the electrode-phase lithium concentration dynamics integrated with fault* (1)–(3)*, and the observer*

in (42)-(44). *For any initial data,* $c_{s,0}^{\pm}(\cdot) \in L^2(0, R_s^{\pm})$,
1) In the absence of fault ($f_s^-(t) = 0$)*, the states of the designed observer converge to the states of the original system in the spatial* L^2 *norm if* $\hat{c}_s^{\pm}(0, r)$ *verifies* (48).
2) In the presence of fault ($f_s^-(t) \neq 0$)*, the estimation error remains bounded if* $\hat{c}_s^{\pm}(0, r)$ *satisfies* (48).

Proof. The stability proof is given in Theorem 1 of [12]. Unlike [12], the surface lithium concentration $c_{\mathrm{ss}}^{+}(t)$ used here is obtained from boundary electrolyte concentrations and voltage inversion, as detailed in Section IV-A. □

The solid phase concentration fault residual signal is defined as the boundary state estimation error [14]:

$$r_{\mathrm{s}}(t) = c_{\mathrm{s}}^{-}(t, R_{\mathrm{s}}^{-}) - \hat{c}_{\mathrm{s},2}^{-}(t, R_{\mathrm{s}}^{-}). \tag{49}$$

The solid-phase threshold level ϵ_{s} is determined in the same manner as the electrolyte-phase threshold.

C. Solid-phase fault estimator

For fault estimation, the solid-phase electrochemical fault term is modeled as $f_{\mathrm{s}}^{-}(t) = \theta_{\mathrm{s}} \bar{\psi}_{\mathrm{s}}(t)$, where θ_{s} represents the unknown fault magnitude and $\bar{\psi}_{\mathrm{s}}(t)$ denotes the known fault component. Using the estimated negative electrode lithium concentration distribution $\hat{c}_{\mathrm{s},1}^{-}(t, r)$ produced by the state observer (42)-(44), the fault estimator is proposed as follows:

$$\frac{\partial \hat{c}_{\mathrm{s},2}^{-}}{\partial t}(t, r) = D_{\mathrm{s}}^{-} \left[\frac{2}{r} \frac{\partial \hat{c}_{\mathrm{s},2}^{-}}{\partial r}(t, r) + \frac{\partial^2 \hat{c}_{\mathrm{s},2}^{-}}{\partial r^2}(t, r) \right] + p_2 \left(c_{\mathrm{s}}^{+}(t, R_{\mathrm{s}}^{+}) - \hat{c}_{\mathrm{s}}^{+}(t, R_{\mathrm{s}}^{+}) \right), \tag{50}$$

$$\frac{\partial \hat{c}_{\mathrm{s},2}^{-}}{\partial r}(t, 0^{-}) = 0, \tag{51}$$

$$\frac{\partial \hat{c}_{\mathrm{s},2}^{-}}{\partial r}(\bar{t}, R_{\mathrm{s}}^{-}) = \frac{I(t)}{D_{\mathrm{s}}^{-} F a_{\mathrm{s}}^{-} L^{-}} + \frac{\hat{\theta}_{\mathrm{s}}(t)\, \bar{\psi}_{\mathrm{s}}(t)}{D_{\mathrm{s}}^{-} F a_{\mathrm{s}}^{-} L^{-}} + \bar{p}_0^{-} \left(c_{\mathrm{s}}^{+}(t, R_{\mathrm{s}}) - \hat{c}_{\mathrm{s}}^{+}(t, R_{\mathrm{s}}) \right), \tag{52}$$

where the estimator gain p_2 will be determined later to ensure the stability of the estimation error system. The unknown fault term is estimated by the following adaptive law:

$$\dot{\hat{\theta}}_{\mathrm{s}}(t) = \frac{1}{k_3} \int_0^1 \bar{\psi}_{\mathrm{s}}(t) \tilde{c}_{s,3}(t, r) dr - \hat{\theta}_{\mathrm{s}}(t) \left\| \tilde{c}_{s,3}(t, r) \right\|, \tag{53}$$

where $k_3 > 0$ and $\tilde{c}_{s,3}^{-}(t, r) \triangleq \hat{c}_{s,2}^{-}(t, r) - \hat{c}_{s,1}^{-}(t, r)$.

Theorem 4. *Consider the electrode-phase lithium concentration dynamics integrated with fault* (1)–(3)*, and the proposed estimator* (50)-(52) *with the update law in* (53)*. If* $k_2 < 1/4$ *and* $k_3 > 0$*, then for any initial data, the distributed state estimation error and the parameter estimation error are ultimately bounded.*

Proof. Consider the Lyapunov function candidate:

$$W_2(t) = \tfrac{1}{2} \left\| \tilde{c}_{\mathrm{s},3}^{-}(t, \cdot) \right\|^2 + \tfrac{k_3}{2} \tilde{\theta}_{\mathrm{s}}^2(t),$$

where $\tilde{\theta}_{\mathrm{s}}(t) = \theta_{\mathrm{s}}(t) - \hat{\theta}_{\mathrm{s}}(t)$. Following the proof of Theorem 2 in [5], stability of the estimation error system can be established. □

V. Fault Isolation

The fault isolation strategy relies on analyzing the estimated fault magnitude to determine whether the fault originates from SEI film growth or lithium plating.

- **Case 1:** If $\hat{\theta}_{\mathrm{e}}(t) \neq 0$ and $\hat{\theta}_{\mathrm{s}}(t) = 0$, the fault is attributed to SEI film growth, since the solid-phase estimator reflects only lithium plating, while the electrolyte-phase estimator captures the combined effects of accelerated SEI film growth and lithium plating.
- **Case 2:** The case $\hat{\theta}_{\mathrm{e}}(t) = 0$ and $\hat{\theta}_{\mathrm{s}}(t) \neq 0$ is physically impossible under the proposed model, because if $\hat{\theta}_{\mathrm{s}}(t) \neq 0$, lithium plating necessarily causes the electrolyte-phase fault magnitude to be non-zero.
- **Case 3:** If both $\hat{\theta}_{\mathrm{e}}(t) \neq 0$ and $\hat{\theta}_{\mathrm{s}}(t) \neq 0$ simultaneously, this represents a more complex scenario and is left for future work.

VI. Simulation

The performance of the fault diagnosis scheme is evaluated through simulations on a $\mathrm{LiFePO_4}$ cell with parameters from Table 1 in [15]. The proposed observers, designed based on the SPMe with modified boundary conditions, are compared with the SPMe with original boundary conditions used as the truth model. The SPMe with original boundary conditions has been shown to closely match the DFN model in [12]. Simulations of the electrolyte-phase fault diagnosis scheme are presented in [5]. The true solid-phase lithium

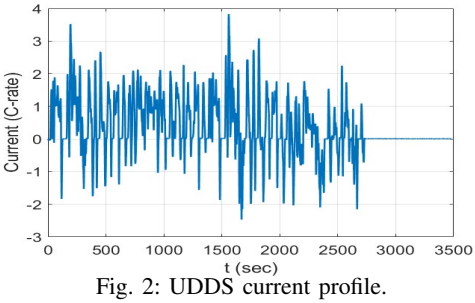

Fig. 2: UDDS current profile.

concentration in the negative electrode, $c_{\mathrm{s}}^{-}(t, r)$, in the absence of fault is shown in Fig. 3, with initial condition $c_{\mathrm{s}}^{-}(0, r) = 1.8244$ kmol/m^3. Fig. 4 illustrates the estimation error of the solid-phase lithium concentration in the fault-free case, where the observer initial condition is $\hat{c}_{\mathrm{s},1}^{-}(0, r) = 1.95$ kmol/m^3. The initial large error, caused by the mismatch between the true and observer initial conditions, decreases and converges over time. To evaluate the performance of the proposed scheme, the following reformulated plating fault function is used for simulation, based on [8]:

$$f_{\mathrm{pl}}^{-}(t, x) = 50 \left(1 - e^{-0.01(t-1000)} \right) e^{0.01x} c_{\mathrm{e}}^{-}(t, L^{-}). \tag{54}$$

The fault is activated at $t = 1000$ s. Fig. 5 shows solid-phase fault detection at the boundary, where the threshold is set to $\epsilon_{\mathrm{s}} = 10$. As shown in Fig. 5, once the residual exceeds the threshold, the fault is detected.

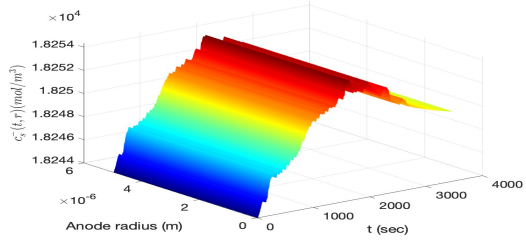

Fig. 3: Solid phase lithium concentration in the negative electrode $c_s^-(t,r)$

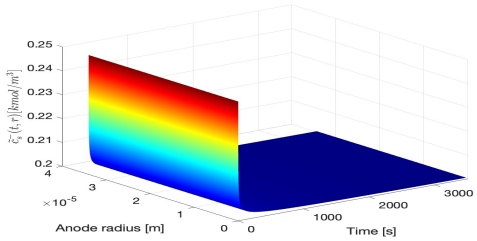

Fig. 4: Estimation error of the solid-phase lithium concentration in the negative electrode in the absence of fault.

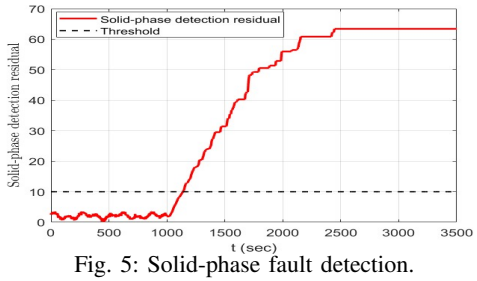

Fig. 5: Solid-phase fault detection.

In Fig. 6, the true and estimated solid-phase fault magnitudes are depicted. The estimation error is ultimately bounded, as confirmed by the results shown in Fig. 6.

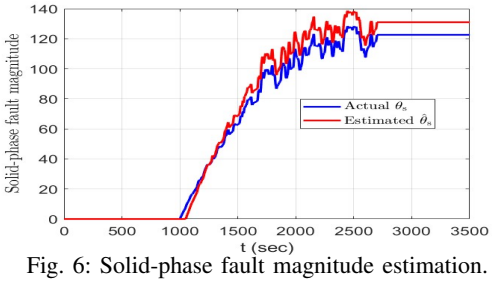

Fig. 6: Solid-phase fault magnitude estimation.

VII. Conclusion and Future Work

In this paper, a model-based fault diagnosis framework for lithium-ion batteries is developed for both the electrolyte and solid phases. Two cascaded PDE backstepping observers are designed. The first observer estimates the distributed lithium concentration and generates a residual for fault detection, while the second observer is activated after detection to quantify the electrochemical degradation fault. A fault isolation strategy exploits the estimated fault magnitudes to distinguish between SEI film growth and lithium plating. Simulation results on a $LiFePO_4$ cell under UDDS current profiles demonstrate that the proposed approach effectively detects and estimates these faults. Future work will extend the framework to additional faults and reversible degradation mechanisms, such as lithium plating dissolution under reverse operating conditions. Future research will also incorporate the temperature-dependent modeling and observer design presented in [16] into the side-reaction models and the proposed fault diagnosis framework.

References

[1] Sadiqa Jafari, Jisoo Kim, and Yung-Cheol Byun. A novel fusion-based deep learning approach with PSO and explainable AI for batteries state of charge estimation in electric vehicles. *Energy Reports*, 12:3364–3385, 2024.

[2] Satadru Dey, Hector E Perez, and Scott J Moura. Model-based battery thermal fault diagnostics: Algorithms, analysis, and experiments. *IEEE Transactions on Control Systems Technology*, 27(2):576–587, 2017.

[3] Hasan Ferdowsi and Sarangapani Jagannathan. Fault diagnosis of a class of distributed parameter systems modeled by parabolic partial differential equations. In *2014 American Control Conference*, pages 5434–5439. IEEE, 2014.

[4] Satadru Dey and Beshah Ayalew. A diagnostic scheme for detection, isolation and estimation of electrochemical faults in lithium-ion cells. In *Dynamic Systems and Control Conference*, volume 57243, page V001T13A001. American Society of Mechanical Engineers, 2015.

[5] Sara Sepasiahooyi and Shu-Xia Tang. Fault diagnosis of electrolyte lithium concentration in lithium-ion batteries. In *Proceedings of the 2025 American Control Conference (ACC)*. IEEE, 2025.

[6] Sara Sepasiahooyi and Shu-Xia Tang. State estimation for lithium-ion batteries based on electrolyte–electrode PDE observers. *Automatica*, 183:112568, 2026.

[7] Sara Sepasiahooyi and Shu-Xia Tang. Enhanced battery state estimation: Part 1-electrolyte lithium-ion concentration observer. In *2024 IEEE 63rd Conference on Decision and Control (CDC)*, pages 3422–3427. IEEE, 2024.

[8] Sara Sepasiahooyi and Shu-Xia Tang. Electrochemical fault diagnosis for lithium-ion batteries: Part 1 – reformulated sei and lithium plating models. In *Proceedings of the 2026 American Control Conference (ACC)*. IEEE, 2026.

[9] Sara Sepasiahooyi and Shu-Xia Tang. Enhanced battery state estimation: Part 2-reverse sensitivity analysis and electrode lithium-ion observer. In *2024 IEEE 63rd Conference on Decision and Control (CDC)*, pages 4251–4256. IEEE, 2024.

[10] Miroslav Krstic and Andrey Smyshlyaev. *Boundary control of PDEs: A course on backstepping designs*. SIAM, 2008.

[11] Hassan K. Khalil. *Nonlinear Systems*. Prentice Hall, Upper Saddle River, NJ, 3rd edition, 2002.

[12] Scott J Moura, Federico Bribiesca Argomedo, Reinhardt Klein, Anahita Mirtabatabaei, and Miroslav Krstic. Battery state estimation for a single particle model with electrolyte dynamics. *IEEE Transactions on Control Systems Technology*, 25(2):453–468, 2016.

[13] Shu-Xia Tang, Leobardo Camacho-Solorio, Yebin Wang, and Miroslav Krstic. State-of-charge estimation from a thermal–electrochemical model of lithium-ion batteries. *Automatica*, 83:206–219, 2017.

[14] Satadru Dey, Hector E Perez, and Scott J Moura. Robust fault detection of a class of uncertain linear parabolic PDEs. *Automatica*, 107:502–510, 2019.

[15] Clément Edouard, Martin Petit, C Forgez, Julien Bernard, and Renaud Revel. Parameter sensitivity analysis of a simplified electrochemical and thermal model for Li-ion batteries aging. *Journal of Power Sources*, 325:482–494, 2016.

[16] Sara Sepasiahooyi and Shu-Xia Tang. PDE state observers for lithium-ion batteries considering temperature effects. In *2026 European Control Conference (ECC)*, page to be appeared. IEEE, 2026.